Low temperature Direct Liquid Injection MOCVD of amorphous CrCx coatings in large-scale reactors: An original route to nanostructured multilayer coatings

Ionela Iliescu, Yoan Gazal, Alexandre Michau, Fouzi Addou, Thomas Duguet, Eric Monsifrot, Frédéric Schuster, Francis Maury

Version of Record: https://www.sciencedirect.com/science/article/pii/S0257897221003480
Manuscript_1f0a585d77ad256f56bcbc8d2faa6a37

Low temperature Direct Liquid Injection MOCVD of amorphous CrC_x coatings in large-scale reactors: an original route to nanostructured multilayer coatings

Ionela Iliescu[1*], Yoan Gazal[1], Alexandre Michau[2], Fouzi Addou[2], Thomas Duguet[1], Eric Monsifrot[3], Frédéric Schuster[4], Francis Maury[1]

[1]*CIRIMAT, CNRS/INPT/UPS, 4 allée E. Monso, 31030 Toulouse, France*

[2]*Université Paris-Saclay, CEA, Service d'Études Analytiques et de Réactivité des Surfaces, 91191, Gif-sur-Yvette, France*

[3]*Dephis, 74 rue Armand Japy, 25460 Etupes, France*

[4]*CEA Cross-Cutting program on Materials & Processes Skills, 91191 Gif-sur-Yvette, France*

*corresponding author:

Dr. Ionela Iliescu

CIRIMAT, ENSIACET, 4 allée E. Monso, BP 44362,

31030 Toulouse cedex, France

Tel.: +33(0)5 34 32 34 41

ionela.iliescu@ensiacet.fr

Authors email address:

yoan.gazal@toulouse-inp.fr

Alexandre.MICHAU@cea.fr

Fouzi.ADDOU@cea.fr

thomas.duguet@toulouse-inp.fr

eric.monsifrot@dephis.com

frederic.schuster@cea.fr

francis.maury@ensiacet.fr

Abstract

The effect of low temperature deposition on the quality and the microstructure of hard *a*-CrC_x coatings grown by Direct Liquid Injection Metal-Organic Chemical Vapor Deposition (DLI-MOCVD) was investigated. At deposition temperatures higher than 525 °C, the coatings are bi-phased and polycrystalline, essentially composed of Cr_7C_3 with Cr_3C_2 as a minor phase. By decreasing the temperature in the 525-350 °C range, they are amorphous and exhibit a monolithic glassy-like microstructure without grain boundary. For temperatures lower than 350 °C, the uniform amorphous microstructure changes for a lamellar multilayer structure, while the composition of the gas phase was kept constant at the inlet of the reactor for all these CVD runs. The origin of this surprising lamellar structure has been investigated. After having discarded the idea of a self-organized multilayer growth, sometimes encountered in CVD processes, evidence was found for rapid changes in the deposition mechanism. They are induced by oscillations of the surface temperature around a critical value due to the regulation of the furnace used for such large-scale reactors. These almost periodic temperature changes lead to modulations in the surface composition of nutrient species, and subsequently, to the growth of multilayers. The individual composition of lamellae changes regularly, while the overall composition of the coatings remains identical to that of uniform monolithic coatings. For growth conditions leading to local temperature close to the critical value, a regular and controlled nanostructuring can be obtained with a period close to a hundred nanometers. Similar to monolithic *a*-CrC_x coatings, these *a*-CrC_x multilayer coatings exhibit a good barrier behavior against high temperature oxidation, according to the test performed. As future prospects, the main interest for these lamellar coatings could be their mechanical properties thanks to the numerous interfaces capable of deflecting and dissipating the propagation of cracks.

Keywords

DLI-MOCVD; Chromium carbide; Low temperature deposition; Protective coatings; Multilayer structure.

1. Introduction

It is well known that a major constraint of industrial CVD processes is the high deposition temperature [1]. For targeted applications, solutions have been found by activating the process, which sometimes becomes hybrid [2-4]. The use of metallorganic precursors is another way to lower the deposition temperatures [5-8]. For instance, carbides and nitrides can be deposited using metallorganic precursors at deposition temperatures several hundred degrees lower. The temperature lowering requires an in-depth study of the structure and properties of coatings to compare them to their high temperature counterparts [7-9]. Another breakthrough for the development of MOCVD processes is the coupling of low temperature sources with the use of high vapor flow rate of precursor, as produced by pulsed Direct Liquid Injection (DLI) system. The DLI-MOCVD process significantly increases its prospects for industrial applications as protective coatings [10]. Specifically, polycrystalline CrC_x coatings deposited at the lab scale at 550 °C either by MOCVD [8] or DLI-MOCVD [11] exhibit comparable composition, structure and growth rate with those produced at about 1050 °C by the halide CVD process (namely, pack cementation [12]). This significant decrease in temperature is due to the greater reactivity of the vapor phase but, consequently, the process scaling can be more complicated. With the aim of developing a large-scale MOCVD process for the deposition of CrC_x as protective metallurgical coatings, a DLI system was connected to a horizontal, stainless steel hot-wall reactor 1 m long [8]. The coatings obtained with this DLI-MOCVD process at 450 °C have a composition close to Cr_7C_3 and a high nanohardness (26 ±3 GPa) [8]. Furthermore, they exhibit a very good resistance to high temperature oxidation in air and steam [13]. As a result, they were used as internal protective coating of 1 m long fuel cladding tubes with 8 mm internal diameter [14]. Both kinetic experimental studies and numerical modeling [15] led to relatively thick coatings with satisfactory thickness uniformity along these narrow tubes. In order to improve the thickness uniformity along the tube, very low temperatures are required. This significantly decreases the reaction

rates in the gas phase, hence, the overall kinetics become dominated by surface reactions. Also, for other applications of CVD process, e.g. infiltration in porous objects for protection in harsh environments [16], conformal and uniform deposition on 3D complex parts, it is necessary to lower the growth temperature as much as possible [17]. For a given chemical system, it is therefore necessary to study carefully the effect of lowering the temperatures to ensure both the properties of the coatings and the viability of the CVD process for different applications.

This paper reports on the influence of the lowest deposition temperatures on the main properties of CrC_x coatings grown by DLI-MOCVD. The composition and structure of these coatings does not change significantly between 525 °C and 350 °C but at 325 °C the growth of a lamellar structure occurs. After a literature review, it was found that it originates from changes in the surface composition induced by temperature oscillations due to the furnace regulation. As promising prospects, the control of the surface temperature will make the process capable of producing nanostructured multilayer *a*-CrC_x coatings with good protective properties.

2. Experimental

2.1. Deposition process

The CrC_x coatings were grown by DLI-MOCVD in a horizontal stainless steel, tubular hot-wall reactor (internal diameter ID 150 mm, length 1300 mm, volume *ca.* 23 L) or directly inside Zircalloy-4 (Zy-4) cladding tubes (ID 8 mm, length 1300 mm) used as a bundle of 16 narrow and long reactors [18]. The particularity of this CVD method is the pulsed injection of very small amounts of a liquid solution kept at room temperature and formed by a viscous precursor diluted in an oxygen-free organic solvent. These micro-droplets are injected with a frequency of 5 Hz in a flash vaporization chamber heated at 180 °C, where the reactive vapor is produced. This vapor is then transported with the aid of an inert carrier gas (N_2) into the reaction zone, where it is thermally decomposed. The deposition takes place either on flat

substrates (Si and metallic alloys coupons) or directly on the inner-wall of the cladding tubes, *i.e.* a concave surface. This DLI-MOCVD process is not only developed for planar surfaces; it can be applied to complex 3D parts, massive or porous, with good conformal coverage and infiltration in porosities, as will be demonstrated in a future paper. A computer controls a Coriolis mass flow meter, the opening time of the injectors and the injection frequency, in order to maintain a constant feed of precursor (0.5 g/min) into the reaction chamber. A 3-zone horizontal tube furnace (Carbolite) equipped with three thermocouples was used; it produces a heating length of 0.9 m and 1200 °C maximum operating temperature. The deposition temperature was set between 325 °C and 525 °C, while the working pressure was set between 0.4 and 2 kPa. For the CrC_x growth, the metallorganic compound bis(ethylbenzene)chromium (BEBC) supplied by Strem Chemicals Inc. was used as precursor. It is commercially available as a mixture of several bis(arene)chromium compounds $[(C_2H_5)_x(C_6H_{6-x})]_2Cr$, with x = 0-4 including approximately 70 mol.% of BEBC, *i.e.* the mono-substituted representative of this family (x=1), while the remaining is a mixture of multi-substituted compounds. Our previous works and that of other authors suggest that all members of this family decompose according to the same mechanism (schematically, release of aromatic ligands starting in the gas phase, heterogeneous decomposition of the aromatic cycles leading to C incorporation into the growing coating). A demonstration of this claim is that direct recycling of effluent in a closed loop produces the same coatings [8]. The BEBC precursor was diluted in toluene solvent (purity 99.8%, Sigma Aldrich) at a total concentration of 0.8 $mol \cdot L^{-1}$. The surface of the samples was cleaned prior to deposition in acetone and ethanol. More details regarding the DLI-MOCVD process can be found in [8, 18].

2.2. Characterization techniques

The crystal structure of the coatings was investigated at room temperature by X-ray diffraction (XRD), in θ−2θ configuration (Bragg-Brentano) with a Bruker D8 Advance diffractometer equipped with a graphite monochromator using $CuK_{\alpha 1+\alpha 2}$ radiation (λ = 1.5419

Å). The data were collected in the 5–90° 2θ range with a scan step of 0.02 and a counting time of 1.5 s per step. Annealing experiments of as-deposited coatings were performed by *in situ* XRD under inert atmosphere (Ar). Different samples were analyzed in the 30–60° 2θ range using a Bruker D8 Advance diffractometer equipped with a LynxEye detector and an MRI radiation heating chamber (Bragg-Brentano configuration; Ni filtered Cu K_α radiation). The XRD chamber was purged with Ar prior to the experiment to remove air traces and the measurements were made under a low Ar flow rate (50 sccm) to maintain an overpressure slightly higher than one atmosphere. The diffractograms were recorded every 50 °C from 500 to 800 °C, except within the temperature range of crystallization 570-680 °C, where the patterns were recorded every 10 °C. An isotherm was maintained at each level to record the XRD pattern, and then the temperature was increased to the next step using a ramp of 5 $°C \cdot min^{-1}$.

The surface morphology and thickness of the coatings were analyzed using a field emission gun scanning electron microscope (FEI QUANTA 450 ESEM FEG). The surface roughness of the coatings was measured using a stylus profiler (DektakXT from Bruker). The overall atomic composition of the coatings was determined by electron probe micro-analysis (EPMA) using a CAMECA SXFive spectrometer (15 kV, 20 nA). Rutherford Backscattering Spectrometry (RBS) was used to estimate the coatings density (1.5 MeV H^+ beam, detection at 160°). For the RBS analysis of the Zy-4 tube samples with concave surface curvatures, an incident ion micro-beam was used to focus a spot of 2 µm in diameter on the sample and the data were extracted from a scan of 500 x 500 µm.

The microstructure of the coatings was studied by transmission electron microscopy (TEM) using a JEOL JEM 2010 microscope operating at 200 kV. For cross-section imaging, the samples were prepared by mechanical polishing, perpendicular to the film surface. The final thinning was performed using the precision ion polishing system (PIPS, Gatan) in order to obtain a large electron transparent area.

A Horiba Jobin Yvon Labram HR 800 spectrometer was used for Raman spectroscopy analysis. Raman spectra were recorded at room temperature in the backscattering micro-Raman mode using a laser light of $\lambda = 514.5$ nm. Typical spectra have been obtained for an acquisition time varying between 240 and 360 s. The Raman bands were fitted with Gaussian profiles using Origin software after baseline subtraction.

One of the novelties of this paper is that most of the results presented originate from analyses (SEM-EDS, XRD, EPMA, RBS, Raman) performed directly on the coatings grown on the inner-wall of long cladding tubes after cutting small sections. No significant difference was found between the coatings on these concave curvature surfaces and those on flat substrates.

3. Results

3.1. Microstructure and composition of CrC_x coatings

CrC_x coatings were deposited on flat substrates (Si wafers and Zy-4 coupons) and directly on the inner-wall of Zy-4 cladding tubes at temperatures between 325 °C and 500 °C with thickness ranging from 1 to 16 µm. They have a metallic mirror-like appearance and a greyish color. All coatings present a very good conformity on the Zy-4 substrates. The surface roughness (Ra) of the coatings measured by profilometry is around 200 ±50 nm, while that of the as-used Zy-4 substrate is around 300 ±50 nm. This reveals a slight smoothing of the surface after deposition. That smoothing is expected for low sticking coefficient conditions, *i.e.* the conditions for conformal growth. The coatings roughness slightly increases with the deposition temperature. Some of the coatings were also deposited on Si substrates with a resulting roughness of about 10 ±2 nm (initial roughness of Si ≤ 1 nm). These low temperature data suggest a good conformal coverage of the CrC_x coating on both surfaces, in agreement with SEM cross sections of samples grown at 450 °C [14].

Fig. 1 shows the cross sectional SEM morphology of the CrC_x coatings grown between 350 and 500 °C (the cross sections were mechanically polished for the observation). The SEM images and the optical inspection indicate that there is no delamination between the coating

and the Zy-4 substrate. All samples present similar features and exhibit a homogenous and dense microstructure with no apparent grain boundaries (glassy-like structure), characteristic of amorphous materials. At deposition temperatures higher than 525 °C (not shown here), the CrC_x coatings are polycrystalline [8]. No apparent inter-diffusion layer is seen at the coating-substrate interface (if present, its thickness is in the nanometric range). It should be noted that the internal surface of the cladding tubes is not perfectly smooth (industrial grade surface) and, because of the small internal diameter (8 mm), an efficient surface preparation (polishing and cleaning) was difficult to implement, except the usual solvent rinsing. For this reason, the presence of a thin oxide layer (< 100 nm), prior to deposition, cannot be completely ruled out, as suggested by TEM observations (not shown here).

The cross sectional SEM morphology of the CrC_x coating grown at 325 °C is shown in Fig. 2 in back-scattered electrons mode (BSE). Interestingly, the microstructure at this very low deposition temperature is different from that of the samples shown in Fig. 1. A dense multilayer structure of alternating grey layers (230-620 nm thick) and thinner dark layers (30-80 nm thick) has grown in a seemingly self-organized mode since the composition of the injected gas phase was not intentionally modulated. A stack of 8 bilayers is observed in this sample through the whole film thickness. The BSE image and the associated concentration profile of Cr, C and Zr elements, indicate a correlation between the opposite small variations of Cr and C and the alternating grey and dark layers. More precisely, the dark thin layers are richer in C (~27 at.%) than the grey thicker layers (~19 at.%) (Fig. 2). However, it is noteworthy that the volume analysed by the EDS probe on this cross-section is bigger than the thickness of the layers, leading to an overlap and a poor vertical resolution.

The atomic composition of CrC_x coatings grown in the 325-500 °C temperature range on the internal surface of the cladding tubes was determined by EPMA and is reported in Table 1. The results show no significant difference between the various samples, within the 1 at.% of the analysis detection limit. The average atomic ratio C/Cr of the CrC_x coatings is 0.49 ±0.05.

This value is intermediate between the stoichiometry of the stable carbides Cr_7C_3 (C/Cr = 0.43) and Cr_3C_2 (C/Cr = 0.67), but closer to Cr_7C_3. Traces of oxygen, coming mainly from the surface contamination of the sample and/or the precursor handling, are below 5 at.%, close to 1-4 at.% values observed by other authors [19].

Because the barrier efficiency of a coating is generally better when its density is high, RBS analyses were performed to investigate the influence of the deposition temperature on the density of the CrC_x coatings. Indeed, it is possible to estimate its density from the atomic density measured by RBS combined with the thickness of the coating measured by SEM and their atomic composition analyzed by EPMA. The data reported in Table 1 indicate that the coatings are dense with a density not far from the theoretical one (within the experimental error). They also show that the deposition temperature has no significant influence on the coatings density and, consequently, the multilayer coating does not differ from this series.

All XRD patterns of the CrC_x coatings grown between 325-500 °C present similar features regardless of the deposition temperature. A typical XRD diffractogram is shown in Fig. 3. There is no evidence of diffraction peaks corresponding to polycrystalline phases, only the presence of broad peaks, characteristic to amorphous/nanocrystalline materials. The broad peaks centered at $2\theta = 42.5°$ and 79° originate from an amorphous chromium carbide phase, since both peaks are centered on the most intense diffraction peaks of the two stable carbides Cr_7C_3 (PDF card 00-036-1482) and Cr_3C_2 (PDF card 00-35-0804) (Fig. 3). According to the Scherrer formula, the correlation length of domains was estimated at *ca.* 2 nm based on the only measurable feature at $2\theta = 42.5°$, which confirms the amorphous character of this carbide phase.

The small broad peak at around $2\theta = 24 \pm 4°$ is assigned to free carbon (free-C). Indeed, it has been reported that the most intense peak of crystallized graphite emerges at $2\theta = 26.5°$ and comes from (002) planes corresponding to the stacking of graphene sheets [20]. However, in our amorphous samples, it can be seen that the 2θ position of this peak is decreasing from

approximately 28° to 20° with the decrease in temperature from 450 °C to 375 °C (Fig. 4a). This behavior can be explained by an increasing degree of disorder of the free-C particles in the CrC_x coatings when lowering the deposition temperature. Many types of C-related defects can occur, which induce a broadening and a shifting of the (002) graphite peak. Most common defects present in carbon containing materials are: turbostratic carbon (rotation and/or translation of graphene planes), disordered stacking of AB graphene layers, increased interlayer spacing at the edges of flakes, bending of graphene layers, and other structural defects [21]. However, in [21] it was shown that the *{00l}* is not influenced by the rotation or the translation of graphene layers because <00l> is the stacking direction of the basal planes. These authors showed that the 2θ shift of the (00*l*) peaks is mainly due to the curvature of the graphene layers. In our case, this could be caused by the insertion of Cr atoms between graphene sheets at the edges of graphite-like flakes, which form a local configuration comparable to that of the molecular precursor, *i.e.* a Cr(0) atom sandwiched between two aromatic ligands. The 2θ decrease of the (002) peak of free-C with the deposition temperature is consistent with the intercalation of Cr atoms at the edges of graphene sheets, which increases the distance between the graphene planes.

By decreasing again the growth temperature from about 350 °C to 325 °C, the 2θ position of this free-C peak increases abruptly and reaches almost the theoretical value of graphite. This could be due to larger graphitic regions without defects in free-C particles which are always present in the amorphous coating grown at 325 °C. This means that the free-C component at 325 °C would be more graphitic than at higher temperatures. This result would be in agreement with the multilayers structure since the dark thin layers in SEM images are richer in C than the grey ones (Fig. 2). In order to quantify the relative amount of free-C compared to the carbidic form of the amorphous CrC_x matrix, the intensity ratio of the peak corresponding to the (002) graphitic planes at 2θ = 24 ±4° and that of the CrC_x matrix at 2θ = 42.5° was plotted against the deposition temperature (Fig. 4b). Two different regions can be

observed: a first one that corresponds to an amorphous nanocomposite structure in the range 450-350 °C where the free-C XRD contribution is low (I_C/I_{CrC} close to 0.1 ±0.1), and a second one in the samples deposited at 325 °C, where the relative content of free-C increases (I_C/I_{CrC} = 0.45 ±0.1). The influence of the deposition temperature shown in Fig. 4 on both the free-C peak position and the ratio I_C/I_{CrC} is consistent with EDS line scan analysis from Fig. 2.

The broad peak at 2θ = 13.8° is assigned to a graphite intercalation compound (GIC) [22, 23] and its origin was discussed in our previous paper [8]. In short, in carbon containing compounds, Cr(0) atoms can be intercalated between two graphene sheets to form sandwich units characterized by η^6-bonds with aromatic rings as in bis(arene)Cr molecular precursor. However, Cr cannot be intercalated between two consecutive AB stacking planes because of the small interplanar space and the shifting between the two sheets. As a result, the corresponding stacking distance of such a locally ordered structure is twice the spacing between two consecutive graphene sheets, *i.e.* 6.556 Å, which corresponds to AA interlayer spaces giving a diffraction angle of 2θ = 13.5°. This is very close to our experimental value of 2θ = 13.8°.

Overall, XRD analysis revealed the amorphous structure of the coatings deposited between 350 and 500 °C and a nanocomposite microstructure comprising free-C particles with more or less defects dispersed in an amorphous chromium carbide matrix. To confirm this result, a CrC_x coating deposited at 400 °C was analyzed by TEM in Fig. 5. The high-resolution image reveals a microstructure composed of dark and bright areas, which indicates regions rich in Cr and C (higher atomic mass and/or denser particles are darker). The black regions are likely Cr-rich and are about 2-3 nm in size, in good agreement with the XRD size estimation of the short-range order in the CrC_x matrix. The lighter areas are smaller, having a size of 1-2 nm. No indication of crystalline order appears in the TEM images suggesting that the sample has a nanocomposite structure consisting of highly disordered free-C domains dispersed in an amorphous chromium carbide matrix *a*-CrC_x.

Nygren et al. [19] obtained similar results regarding the crystallinity state of as-deposited Cr-C films grown by reactive magnetron sputtering. Also, a microstructure consisting of black and bright areas assigned to Cr-rich and C-rich phases, respectively, was reported in [24] as in our TEM image (Fig. 5).

As described below, Raman provides some detailed insight, consistent with the XRD and TEM results. As for these techniques, the Raman bands are often interpreted with reference to crystalline phases, although their width is characteristic of an amorphous state. Typical Raman spectra of CrC_x coatings are shown in Fig. S1. The spectra present broad bands indicating that the coating is amorphous in nature. Two regions can be distinguished in the 100-1800 cm^{-1} spectral range. The first one, below 1000 cm^{-1}, is characteristic of chromium oxides (Cr_2O_3, CrO_2), which form as a very thin layer contaminant at the surface of the samples. No relevant information of the coating is found in this region.

The presence of the second region shown in Fig. 6 (1000-1800 cm^{-1}) is essentially due to different carbonaceous species present in the coatings. The deconvolution of the bands in this region reveals the coexistence of 4 modes: D and G bands representative of the C-C bonds, TPA1 and TPA2 of trans-polyacetylene assigned to C=C chain stretching and CH wagging modes [25]. The small band marked as (*) was not assigned because the very narrow shape feature is incoherent with the amorphous structure of the coatings already highlighted by XRD and TEM. In addition, its presence was not systematic and unrelated to the growth conditions.

Often in C-containing materials, the trans-polyacetylene peaks at about 1215 (TPA1) and 1445 cm^{-1} (TPA2) appear together and can be assigned to the n1 and n3 molecule vibration modes, which correspond to the sum and different combinations of C=C chain stretching and CH wagging modes. Although these bands are quite intense compared to the D and G bands, the relative amount of TPA may be very small due to the high Raman cross section of TPA [25].

The D-mode found at 1340±5 cm^{-1} is a breathing mode of A_{1g} symmetry that becomes active in the presence of disordered graphite (in perfect graphite, it is forbidden). Its intensity is related to the presence of sixfold aromatic rings. The G-mode at 1595±20 cm^{-1} has E_{2g} symmetry and comes from the in-plane bond stretching motions of sp^2 C atoms. This mode can occur at all sp^2 sites and does not strictly require the presence of sixfold aromatic rings [26]. Therefore, both D and G are common to sp^2-hybridized carbon [27].

It is well known from the Tuinstra-Koenig equation [28] that the intensity ratio I_D/I_G of D and G bands correlates with the crystallite size (*i.e.* in-plane correlation length or graphitic cluster diameter) by the derived relation: $I_D/I_G = A/L_a$, where L_a is the crystallite size and A is a constant for a fixed laser excitation energy (in our case A=19 for E_L=2.33 eV [29]). However, Ferrari and Robertson [26] showed that when the value of L_a is below 2 nm, as indicated by our XRD and TEM data, the Tuinstra-Koenig equation is no longer valid. Indeed, Fig. 7 shows similar results to that obtained by Ferrari et al. when plotting the variation of the I_D/I_G ratio with L_a. This suggests that by lowering the deposition temperature, a transition between amorphous carbon (a-C) and nanocrystalline graphite (nc-G) occurs at around T=325 °C following the three stage amorphization trajectory proposed by Ferrari [26]. Thus, at low temperatures there is a tendency of forming disordered nc-G (aromatic clusters, sp^2 C with point and linear defects), while towards 450 °C the tendency is to form *a*-C (C domains with less and less aromatic clusters et more other types of defects such as sp^3). In addition, we have plotted in Fig. 8 the G band position σ_G vs. its width Γ_G and compared our data with those for nc-G and different *a*-C reported by Merlen et al. [27]. It can be observed that at high deposition temperature our data are close to the literature data for *a*-C, while below 350 °C the data tend towards the nc-G region. These findings are consistent with the XRD results, which indicated a more graphitic free C component, both at 325 °C and at high T, but after going through a lower degree of graphitization (Fig. 4a). These results show that the other techniques are consistent with the greater insight provided by Raman spectroscopy.

3.2. Thermal stability of CrC coatings

In order to study the thermal stability of as-deposited coatings and the crystallization temperatures of different phases, *in situ* XRD analyses were performed in Ar atmosphere from RT to 800 °C for two samples deposited at 350 °C and 500 °C. The series of XRD patterns shown in Fig. S2 allowed determining the crystallization temperatures given in Table 2.

For the sample grown at 500 °C, which exhibits an amorphous nanocomposite structure, the first phase that crystallizes is Cr_7C_3 (575 °C), rapidly followed by Cr_3C_2 (590 °C). Then, traces of contaminating oxide (Cr_2O_3) crystallize at about 610 °C. This oxide may originate from traces of oxygen in as-deposited coatings (< 5 at.%) or from the *in situ* XRD chamber during annealing (insufficient purging or air-leaks). All these phases are stable up to 800 °C (the highest investigated temperature). The crystallization temperatures of the carbide phases are in good agreement with the crystallization temperature of ~580 °C reported for Cr-C films deposited by RF magnetron sputtering with a C composition close to 30 at.%, *i.e.* close to the Cr_7C_3 stoichiometry [30].

For the amorphous coating deposited at 350 °C, both stable carbides Cr_7C_3 and Cr_3C_2 crystallize at 525 °C (Table 2). Although this coating was grown with a furnace set point of 350 °C, the sample analyzed was located near the extremities of the reactor, where the local temperature was close to 325 °C. Thus, this as-deposited amorphous coating exhibits a multilayer structure. Interestingly, similar to the coatings grown at T > 350 °C, the crystallization temperature of Cr_2O_3 traces does not change, *ca.* 615 °C. However, the crystallization temperature of the carbide phases is about 50 °C lower compared to that of uniform amorphous coatings as-grown at T > 350 °C. This suggests that the crystallization of the two carbides is easier for lamellar coatings than for those with a monolithic structure. This would be consistent with the fact that in the multilayer coating, each layer would have a

composition very close to that of the two stable carbides, *i.e.* the light grey layers would be *a*-Cr_7C_3 and the dark layers *a*-Cr_3C_2.

3.3. Barrier to high temperature oxidation of multilayers

The behavior of the coated Zy-4 sample grown at 325 °C with a multilayered structure was studied by heating the sample under Ar at 550 °C for 4 h, followed by heating it at 1100 °C for 15 min in ambient air, and then, quenched in water at RT. This procedure was previously applied for other protective coatings in order to simulate an accidental event such as the loss of coolant in the primary circuit of a nuclear power plant [13, 18, 31]. The preliminary results reported here indicate promising oxidation resistance at high temperature and in corrosive environment (Fig. 9). The multilayer structure behaves similarly to the samples deposited at temperatures higher than 325 °C (which have a monolithic structure), for instance those grown at 450 °C [13]. No significant difference was found between the two structures. This lamellar microstructure withstands abrupt heat treatment, without change in the multilayer structure and the relative thicknesses of the individual layers (still visible after the test). Some porosities appear mainly pinned at the coating/substrate interface (black spots in zone 3 of Fig. 9). The cross-section images reveal cracks perpendicular to the sample surface penetrating through the film thickness, but quite rarely up to the interface with the substrate. Some of them may come from the sample preparation for observation. When there is a through crack, the onset of oxidation of the Zy-4 substrate is observed at the bottom of the cracks (zone 4 in Fig. 9).

The EDS analysis of the sample performed after the heating to 1100 °C and quenching indicates that the main part of the CrC_x coating has the same composition as prior to the oxidation treatment: the C content at the points 1 and 2 of Fig. 9 is approximately 28 at.%, which is very close to EPMA data in Table 1. An interdiffusion layer containing C, Cr and Zr has formed at the interface with the Zy-4 substrate (point 3), likely because of the migration of Zr into the coating. Also, an intermediate layer, due essentially to the C diffusion into the

Zy-4 substrate, forms an irregular and continuous interdiffusion sublayer generating probably ZrC and containing oxygen, as well as an intensified oxidation at the bottom of a through crack (point 4 in Fig. 9).

4. Discussion

The morphology, microstructure and composition of the CrC_x coatings deposited at temperatures between 350-500 °C are very similar. Furthermore, SEM, TEM and XRD analyses showed evidence of an amorphous nanocomposite structure made of a CrC_x matrix and disordered free-C regions with a more or less extended interphase domain depending on the deposition temperature as suggested by Raman analysis. The only significant difference was found for the samples deposited at 325 °C. Basically, SEM-EDS reveals that these low temperature coatings present an unexpected multilayer microstructure composed of alternating dark and bright layers, where the C content oscillates by a few percent between the high and low values, respectively. Generally, both types of microstructure (dispersed nanocomposite and multilayer) present superior properties compared to uniform polycrystalline Cr-C coatings. For instance, Nygren et al. [19] showed that an amorphous X-ray nanocomposite formed by *a*-CrC_x and *a*-C had the highest overall oxidation resistance. By eliminating the grain boundaries, the amorphous materials are excellent candidates for corrosion resistance compared to their crystalline counterparts. In the following discussion, we will focus on *(i)* better explaining the microstructural aspects of our films, and *(ii)* on the origin of the lamellar structure.

4.1. Is this nanostructuring governed by a self-organized mechanism?

Since the CVD parameters were not intentionally varied (mainly the initial composition of the gas phase and the furnace temperature), one of the possible origin of a lamellar structure in CVD may be a self-organized multilayer growth as reported for the ternary system Ti-Al-N [32, 33]. Keckes *et al.* [33] reported the spontaneous formation of TiAlN multilayers made of periodically alternating cubic TiN and hexagonal AlN nanolamellae. The multilayer features

were nano-sized, randomly oriented and confined in polycrystalline micron-size grains, which is very different from the fully lamellar microstructure of our coatings. These authors have proposed two mechanisms for the formation of the lamellar structures. First, they presumed that the lamellae formed already during the CVD growth as a result of high deposition rates (5 μm/h), allowing only short diffusion lengths. Concomitantly, due to the high temperature, the growth occurred close to the thermodynamic equilibrium and the phase separated via surface diffusion that is kinetically favored compared to bulk diffusion. This mechanism does not hold for our DLI-MOCVD process that is strongly kinetically controlled. As second route, they supposed that the growth of the lamellae could be due to kinetically controlled oscillating surface reactions. It would be energetically favorable to form one of the phases before the second one nucleates. For example, this kinetically controlled route was reported in CVD of Ti(C,N) multilayer coatings using various hydrocarbons precursor of different reactivities, which leads to temporal instabilities on the growing surface [34]. The formation of lamellar structures by this mechanism is interesting for our MOCVD process but it cannot be retained since we only use one type of C source (aromatic ligands of the BEBC precursor) and not an aromatic/aliphatic mixture with different reactivity by contrast with [34], and our deposition temperature is considerably lower than the 800 °C used in [33].

Nano-lamellar $Al_{0.8}Ti_{0.2}N$ coatings that consist of alternating only cubic phases were also deposited by LPCVD at 800 °C using halide precursors [32]. In addition to growth kinetics, an epitaxial relationship between fcc-Ti-rich and fcc-Al-rich lamella was one of the causes that stabilized this self-organized microstructure. In our case, epitaxial relationship cannot be considered since the lamellae are amorphous and probably much thicker than what would stabilize the phases.

Since the average composition of our multilayer coatings is intermediate between the Cr_7C_3 and Cr_3C_2, the hypothesis of a demixing of the amorphous *a*-CrC_x phase into these stable phases was also considered. One layer would be richer in C than the other, similar to

explanation proposed in [35, 36] for CVD grown TiAlN coatings. However, this idea was quickly discarded because the as-deposited multilayer coatings grown at 325 °C are thermally stable up to about 525 °C (crystallization) and their multilayer microstructure is preserved up to 1100°C.

There are also some reports on the controllable preparation of self-organized nano-multilayered structures in M-C films (M = Cr, Cu, Ni, Pt, Ti) grown mainly by PVD [37-40]. However, the mechanisms were not well understood and they are not appropriate for CVD processes, since, for instance, the effects of re-sputtering could be one of the causes of self-organization [40].

In MOCVD processes, the formation of nanolamellar microstructure was reported in the Al-Zr-Y-O system. However, the lamellae were not formed by a self-organized mechanism but they were due to the use of a screw feeder for precursor powder delivery, which induced a pulsed precursor feeding leading to fluctuations in the precursor delivery [41]. Nash *et al.* [42] reported in 1968 the first example of lamellar CrC_x coatings grown by MOCVD starting with bis(benzene)chromium as precursor (the parent compound of the bis(arene)Cr family). They only found a little difference in the C content of the different layers and the origin of this structure was not commented [42]. Later, also using a bis(arene)Cr precursor, Bryskin *et al.* [43, 44] have reported a layered structure in MOCVD chromium carbide coatings, characterized by the alternation of chromium and chromium carbide layers with high-carbon interlayer, but again no explanation for the growth mechanism was given. At this stage, even if a multilayer growth was observed in MOCVD of CrC coatings it has not been demonstrated that this is the result of a self-organized mechanism. Moreover, the most convincing examples (which generally concern ternary systems) and the proposed mechanisms do not seem suitable for our MOCVD process.

Since the early 90s we have published many papers on MOCVD of Cr-based coatings by employing various bis(arene)Cr as precursors and using different evaporation systems

(sublimation, bubbler, DLI) and lab-scale reactor configurations (hot- and cold-wall, horizontal and vertical reactors, atmospheric and low pressure) but we have never observed a lamellar growth. Obviously, nanostructured multilayer Cr-based coatings can be deposited by this DLI-MOCVD process by acting on the parameters, precisely by monitoring the gas phase composition [45]. In fact, we have never studied the growth at temperature as low as 325 °C using precursor of the bis(arene)Cr family prior to working with large-scale MOCVD reactors and simultaneously aiming for lower temperatures to improve thickness uniformity, conformal coverage and infiltration into porous objects. Consequently, taking into consideration this short literature review and the present experimental results, we have investigated the origin of our unusual lamellar microstructure by analysing in more detail the local deposition conditions.

4.2. Proposed mechanism for nanostructured multilayer growth

One of the most important parameters in MOCVD is the growth temperature. We have measured the variation of the deposition temperature along the tubular furnace and its temporal variation. The results are shown in Fig. 10. It can be observed that under CVD conditions and for a given set point of 325 °C on the furnace, the temperature profile as function of the position along the 90 cm reactor (Fig. 10a) presents a steep variation at the extremities of the heating zone. The isothermal zone is approximately 60 cm long, with an average temperature of 333 °C. This is slightly higher than the set point of 325 °C. Furthermore, at the beginning of the isothermal zone, typically at about 10 cm from the entrance into the reactor, the temporal variation of the local temperature exhibits irregular oscillations with a period of about 10 min and extreme values between 325 °C and 360 °C (Fig. 10b). This large temperature amplitude is generated by the PID (Proportional-Integral-Derivative) controller of the furnace, which is not well adapted for such very low working temperatures. These local temperature variations indicate that different reaction mechanisms may produce the growth of the CrC_x coating.

The reaction pathways that lead to the formation of CrC_x coating starting from the BEBC precursor (and more generally from bis(arene)Cr) were already discussed in terms of homogeneous gas phase and surface reactions generating Cr and C nutrient species for the growth of the coating [15]. These reaction pathways are summarized in Table S1. From this relatively simple overall chemical mechanism we propose that at the lowest temperatures (<350 °C) a change in the kinetic mechanism occurs, almost periodically depending on the local temperature, by alternatively activation and extinction of certain elementary reactions. The oscillation of these reactions would produce significantly different concentrations of C sources on the surface leading to an almost regular modulation of the C content in the growing layer. The trigger for the alternating growth could be the temporal fluctuations of the temperature around the set point of 325 °C. In this kinetic mechanism, a key elementary reaction would be the dissociative adsorption of BEBC molecules (reaction #5 in Table S1), which is favored at low temperature. At temperature higher than 350 °C, the BEBC molecules would be totally consumed by a homogeneous gas phase decomposition producing mono(arene)Cr intermediates (reaction #1 in Table S1). As a result, for T > 350 °C, the reaction #5 and subsequently the associated reaction #6 were neglected in the reduced chemical mechanism used in the process modeling [15]. In this simplified mechanism based only on reactions #1 to #4, which was found valid for T > 350 °C, all the C incorporated in the growing layer would originate from the heterogeneous decomposition of one aromatic ligand (reaction #3 in Table S1). By contrast, for T ≤ 350 °C, the heterogeneous decomposition of the mono(arene)Cr intermediate (reaction #6) directly coming from the dissociative adsorption of BEBC (reaction #5) would be another source of adsorbed aromatic ligand, which will lead also to C incorporation into the film by the reaction #3. As a result, the C content of coatings grown at the lowest temperatures should be higher than that of coatings deposited at high temperature. This is in agreement with our experimental results.

After a better setting of the furnace PID for low temperatures, the local temperature in the

center of the isothermal zone (surrounded by a blue circle in Fig. 10) exhibits more regular oscillations in a lower temperature range around 333 °C as mean value (see Fig. 11a). The period of these oscillations is about 7 min and the amplitude is ranging from 328 °C to 340 °C, slightly higher than the set point value, but a better regularity is observed compared to the end zone. In this spatial region, where the period of the oscillations is almost constant (Fig. 11a), the thicknesses of the individual layers are more regular, as shown on the cross-section of a coating on Zy-4 substrate (Fig. 11b). It can be seen that the multilayer structure is correlated with the temperature changes generated by the PID controller of the furnace. The multilayer nanostructuring of this 11 µm thick *a*-CrC_x coating is better controlled and more regular, with a bilayer period of approximately 600 nm.

This demonstrates a new potential of this DLI-MOCVD process for producing nanostructured multilayer coatings by controlling the substrate temperature instead of the composition of the reactive gas phase that continuously change along a large-scale reactor. Obviously, this cannot be applied to any chemical system, but the chemical mechanism used here can possibly be extended to the deposition of other metal carbides (M = V, Nb, Cr, Mo, W) already deposited using bis(arene)M precursors, and which are important metallurgical protective coatings.

5. Conclusions

We have deposited amorphous chromium carbide coatings by DLI-MOCVD at temperatures between 325-500 °C on different types of substrates by focusing on the growth at the lowest temperatures. Two horizontal large-scale hot-wall reactors were used. Various 2D substrates were placed inside a large tubular stainless steel reactor, 1.3 m long (ID 150 mm). The growth was also directly performed on the inner-wall of 1.3 m long Zy-4 cladding tubes using specific flanges to simultaneously process a bundle of 1 to 16 cladding tubes per MOCVD run [18]. The role of the deposition temperature on the coatings microstructure was investigated. For temperatures higher than 525 °C, the coatings are polycrystalline and biphasic, with Cr_7C_3

as the dominant phase and Cr_3C_2 as the secondary one. In the 525-350 °C temperature range, they are amorphous, without grain boundary, thus exhibiting a dense, monolithic and glassy-like structure. At the nanometric scale, they can be described as amorphous nanocomposite coatings composed of disordered free-C nanoparticles embedded in an amorphous carbide matrix with a composition close to *a*-Cr_7C_3, which leads to an overall C content of about 33 at.%, *i.e.* intermediate between the stable carbides Cr_7C_3 and Cr_3C_2.

At the low temperature of 325 °C, the amorphous coatings exhibit an unexpected multilayer architecture, where the atomic C composition is modulated by a few percent. After having discarded several hypotheses to explain the formation of this nano-lamellar microstructure, it was found that it was due to the temporal variations of the local growth temperature, which can be significantly and periodically different from the setpoint of the furnace in a large-scale reactor. The chemical mechanism previously reported [15] suggests that this lamellar structure would result from the activation and deactivation of elementary reactions leading to a quasi-regular modulation of the nature and content of the nutrient C species on the surface and, consequently, on the C incorporation into the growing layer. The lamellar structure grown at 325 °C is unusual and specific to this chemical system used in DLI-MOCVD. Therefore, monitoring more carefully the growth temperature around this critical temperature of 325 °C allows to control this alternating growth. Interestingly, these lamellar coatings exhibits a good thermal stability and an oxidation barrier behavior as good as that of the amorphous monolithic *a*-CrC_x coatings [13], with the advantage of being deposited at a lower temperature. Indeed, it is shown in a companion paper that inner multilayer *a*-CrC_x coatings of cladding tubes provide a good protection against both steam oxidation at 1200°C and secondary hydriding after Zy-4 clad ballooning and burst [31]. Other physical properties, in particular mechanical, must be studied to evaluate the performances of these interface-controlled microstructures for practical applications.

Acknowledgements

The authors thank Cédric Charvillat and Olivier Marsan for their help in XRD and Raman measurements, along with Michaël Ougier for thermal treatments and scanning electron observations. The authors also thank The Raimond Castaing Microanalysis Centre, Toulouse, France, for TEM and EPMA analyses as well as ARCANE-CENBG, Gradignan, France, for RBS measurements. This work was supported by the CEA-CNRS-INPT under Grand No. CV2016-047.

Appendix A. Supplementary data

Supplementary data associated with this article can be found in the online version at https://doi.org/...

References

[1] H. O. Pierson, Handbook of chemical vapor deposition. Principles, technology and applications, William Andrew 2nd Edition (1999)

[2] Y. Li, D. Mann, M. Rolandi, W. Kim, A. Ural, S. Hung, A. Javey, J. Cao, D. Wang, E. Yenilmez, Q. Wang, J.F. Gibbons, Y. Nishi, H. Dai, Preferential growth of semiconducting single-walled carbon nanotubes by a plasma enhanced CVD method, Nano Letters 4, 2 (2004) 317-321, https://doi.org/10.1021/nl035097c

[3] Q. Fang, J.-Y. Zhang, Z. Wang, M. Modreanu, B.J. O'Sullivan, P.K. Hurley, T.L. Leedham, D.Hywel, M.A. Audier, C. Jimenez, J.-P. Senateur, I.W. Boyd, Interface of ultrathin HfO_2 films deposited by UV-photo-CVD, Thin Solid Films 453–454 (2004) 203-207, https://doi.org/10.1016/j.tsf.2003.11.186

[4] T. Wang, H.W. Xin, Z.M. Zhang, Y.B. Dai, H.S. Shen, The fabrication of nanocrystalline diamond films using hot filament CVD, Diam. Relat. Mater. 13 (2004) 6–13, https://doi.org/10.1016/j.diamond.2003.08.014

[5] F. Maury, Trends in precursor selection for MOCVD, Chem. Vap. Deposition 2 (1996) 113-116, https://doi.org/10.1002/cvde.19960020306

[6] S.E. Koponen, P.G. Gordon, S.T. Barry, Principles of precursor design for vapour deposition methods, Polyhedron 108 (2016) 59–66, https://doi.org/10.1016/j.poly.2015.08.024

[7] F. Maury, L. Gueroudji, C. Vahlas, Selection of metalorganic precursors for MOCVD of metallurgical coatings: application to Cr-based coatings, Surf. Coat. Technol. 86–87 (Part 1) (1996) 316–324, https://doi.org/10.1016/S0257-8972(96)03045-9

[8] A. Michau, F. Maury, F. Schuster, R. Boichot, M. Pons, E. Monsifrot, Chromium carbide growth at low temperature by a highly efficient DLI-MOCVD process in effluent recycling mode, Surf. Coat. Technol. 332 (2017) 96–104, https://doi.org/10.1016/j.surfcoat.2017.06.077

[9] A. Billard, F. Maury, P. Aubry, F. Balbaud-Célérier, B. Bernard, F. Lomello, H. Maskrot, E. Meillot, A. Michau, F. Schuster, Emerging processes for metallurgical coatings and thin films, C. R. Phys. 19 (2018) 755–768, https://doi.org/10.1016/j.crhy.2018.10.005

[10] V. Astié, C. Millon, J.-M. Decams, A. Bartasyte, Chemical vapor deposition for nanotechnology, chapter Direct liquid injection chemical vapor deposition, Pietro Mandracci, IntechOpen (2018), DOI: 10.5772/intechopen.80244

[11] F. Schuster, F. Lomello, F. Maury, A. Michau, R. Boichot, M. Pons, Nuclear component with amorphous CrC coating, method for the production thereof by DLI-MOCVD, and uses of same for controlling oxidation/hydridation, United States Patent Application 20200035369 (2020)

[12] S.D. Cramer, B.S. Covino Jr., ASM Handbook Volume 13A: Corrosion: Fundamentals, testing, and protection, ASM International (2003) 763–771

[13] A. Michau, F. Maury, F. Schuster, F. Lomello, J.-C. Brachet, E. Rouesne, M. Le Saux, R. Boichot, M. Pons, High-temperature oxidation resistance of chromium-based coatings deposited by DLI-MOCVD for enhanced protection of the inner surface of long tubes, Surf. Coat. Technol. 349 (2018) 1048-1057, https://doi.org/10.1016/j.surfcoat.2018.05.088

[14] A. Michau, F. Maury, F. Schuster, F. Lomello, R. Boichot, M. Pons, J.-C. Brachet, E. Monsifrot, Inner-side coatings for advanced fuel claddings processed by DLI-MOCVD, Proceedings of Water Reactor Fuel Performance Meeting (WRFPM) (2017)

[15] A. Michau, F. Maury, F. Schuster, I. Nuta, Y. Gazal, R. Boichot, M. Pons, Chromium carbide growth by direct liquid injection chemical vapor deposition in long and narrow tubes, experiments, modeling and simulation, Coatings 8(220) (2018) 1-19, https://doi.org/10.3390/coatings8060220

[16] P. Delhaes, Chemical vapor deposition and infiltration processes of carbon materials, Carbon 40 (2002) 641–657, https://doi.org/10.1016/S0008-6223(01)00195-6

[17] J.R. Abelson, G. S. Girolami, New strategies for conformal, superconformal, and ultrasmooth films by low temperature chemical vapor deposition, J. Vac. Sci. Technol. A 38, 030802 (2020), https://doi.org/10.1116/6.0000035

[18] A. Michau, Y. Gazal, F. Addou, F. Maury, T. Duguet, R. Boichot, M. Pons, E. Monsifrot, H. Maskrot, F. Schuster, Scale up of a DLI-MOCVD process for the internal treatment of a batch of 16 nuclear fuel cladding segments with a CrC_x protective coating, Surf. Coat. Technol. 375 (2019) 894–902, https://doi.org/10.1016/j.surfcoat.2019.06.101

[19] K. Nygren, M. Andersson, J. Högström, W. Fredriksson, K. Edström, L. Nyholm, U. Jansson, Influence of deposition temperature and amorphous carbon on microstructure and oxidation resistance of magnetron sputtered nanocomposite Cr-C films, Appl. Surf. Sci. 305 (2014) 143–153, https://doi.org/10.1016/j.apsusc.2014.03.014

[20] A. Sayah, F. Habelhames,A. Bahloul, B. Nessark, Y. Bonnassieux, D. Tendelier, M. El Jouad, Electrochemical synthesis of polyaniline-exfoliated graphene composite films and their capacitance properties, J. Electroanal. Chem. 818 (2018) 26-34, https://doi.org/10.1016/j.jelechem.2018.04.016

[21] Z.Q. Li, C.J. Lu, Z.P. Xia, Y. Zhou, Z. Luo, X-ray diffraction patterns of graphite and turbostratic carbon, Carbon 45 (2007) 1686-1695, https://doi.org/10.1016/j.carbon.2007.03.038

[22] J. Xu, Y. Dou, Z. Wei, J. Ma, Y. Deng, Y. Li, H. Liu, S. Dou, Recent progress in graphite intercalation compounds for rechargeable metal (Li, Na, K, Al)-ion batteries, Adv. Sci. 4(10) (2017) 1700146 1-14, https://doi.org/10.1002/advs.201700146

[23] M.S. Dresselhaus, G. Dresselhaus, Intercalation compounds of graphite, Adv. Phys. 51 (2002) 1-186, https://doi.org/10.1080/00018730110113644

[24] K. Nygren, M. Samuelsson, A. Flink, H. Ljungcrantz, Å. Kassman Rudolphi, U. Jansson, Growth and characterization of chromium carbide films deposited by high rate reactive magnetron sputtering for electrical contact applications, Surf. Coat. Technol. 260 (2014) 326–334, https://doi.org/10.1016/j.surfcoat.2014.06.069

[25] R. García-Calzada, M. Rodio, K. Bagga, R. Intartaglia, P. Bianchini, V.S. Chirvony, J.P. Martínez-Pastora, Facile laser-assisted synthesis of inorganic nanoparticles covered by a carbon shell with tunable luminescence, RSC Adv. 5 (2015) 50604-50610, https://doi.org/10.1039/C5RA07319G

[26] A.C. Ferrari, J. Robertson, Interpretation of Raman spectra of disordered and amorphous carbon, Phys. Rev. B 61 (2000) 14095-14107, https://doi.org/10.1103/PhysRevB.61.14095

[27] A. Merlen, J. Buijnsters, C. Pardanaud, A guide to and review of the use of multiwavelength Raman spectroscopy for characterizing defective aromatic carbon solids: from graphene to amorphous carbons, Coatings 7 (10) 153 (2017) 1-55, https://doi.org/10.3390/coatings7100153

[28] F. Tuinstra, J.L. Koenig, Raman spectrum of graphite, J. Chem. Phys. 53 (1970) 1126-1130, https://doi.org/10.1063/1.1674108

[29] P. Puech, M. Kandara, G. Paredes, L. Moulin, E. Weiss-Hortala, A. Kundu, N. Ratel-Ramond, J.-M. Plewa, R. Pellenq, M. Monthioux, Analyzing the Raman spectra of graphenic carbon materials from kerogens to nanotubes: what type of information can be extracted from defect bands?, C 5, 69 (2019) 1-20, https://doi.org/10.3390/c5040069

[30] E. Bauer-Grosse, Thermal stability and crystallization studies of amorphous TM–C films, Thin Solid Films 447-448 (2004) 311–315, https://doi.org/10.1016/S0040-6090(03)01108-8

[31] J. C. Brachet, S. Urvoy, E. Rouesne, G. Nony, M. Dumerval, M. Le Saux, F. Ott, A. Michau, F. Schuster, F. Maury, DLI-MOCVD Cr_xC_y coating to prevent Zr-based cladding from inner oxidation and secondary hydriding upon LOCA conditions, J. Nucl. Mater. 550 (2021) 152953, https://doi.org/10.1016/j.jnucmat.2021.152953

[32] J. Todt, J. Zalesak, R. Daniel, R. Pitonak, A. Köpf, R.Weißenbacher, B. Sartory, C. Mitterer, J. Keckes, Al-rich cubic $Al_{0.8}Ti_{0.2}N$ coating with self-organized nano-lamellar microstructure: Thermal and mechanical properties, Surf. Coat. Technol. 291 (2016) 89–93, https://doi.org/10.1016/j.surfcoat.2016.02.027

[33] J. Keckes, R. Daniel, C. Mitterer, I. Matko, B. Sartory, A. Koepf, R.Weißenbacher, R. Pitonak, Self-organized periodic soft-hard nanolamellae in polycrystalline TiAlN thin films, Thin Solid Films 545 (2013) 29–32, https://doi.org/10.1016/j.tsf.2013.08.001

[34] K. Bartsch, A. Leonhardt and E. Wolf, Deposition of multilayer hard coatings using kinetically controlled chemical vapour deposition processes, Surf. Coat. Technol. 54/55 (1992) 193-197, https://doi.org/10.1016/S0257-8972(09)90049-4

[35] F. Uny, S. Achache, S. Lamric, J. Ghanbaja, E. Fischer, M. Pons, E. Blanquet, F. Schuster, F. Sanchette, Deposition and characterization of (Ti,Al)N coatings deposited by thermal LPCVD in an industrial reactor, Surf. Coat. Technol. 358 (2019) 923-933, https://doi.org/10.1016/j.surfcoat.2018.12.014

[36] P. H. Mayrhofer, Self-organized nanostructures in the Ti–Al–N system, Appl. Phys. Lett. 83 (2003) 2049-2051, https://doi.org/10.1063/1.1608464

[37] W.-Q. Wang, L. Ji, H.-X. Li, X.-H. Liu, H.-D. Zhou, J.-M. Chen, Controllable fabrication of self-organized nano-multilayers in copper–carbon films, Chin. Phys. B 28 (2019) 036802 1-8, https://doi.org/10.1088/1674-1056/28/3/036802

[38] W.-Y. Wu, J.-M. Ting, Self-assembled alternating nano-scaled layers of carbon and metal, Chem. Phys. Lett. 388 21 (2004) 312-315, https://doi.org/10.1016/j.cplett.2004.03.004

[39] C.Q. Chen, Y.T. Pei, K.P. Shaha, J.T.M. De Hosson, Tunable self-organization of nanocomposite multilayers, Appl. Phys. Lett. **96** (2010) 073103 1-3, https://doi.org/10.1063/1.3318262

[40] P.E. Hovsepian, Y.N. Kok, A.P. Ehiasarian, R. Haasch, J.-G. Wen, I. Petrov, Phase separation and formation of the self-organised layered nanostructure in C/Cr coatings in conditions of high ion irradiation, Surf. Coat. Technol. 200 (2005) 1572 – 1579, https://doi.org/10.1016/j.surfcoat.2005.08.095

[41] N.K. Eils, P. Mechnich, H. Keune, G. Wahl, C.-P. Klages, Single-step fabrication of nanolamellar structured oxide ceramic coatings by metal-organic chemical vapor deposition; J. Nanosci. Nanotechnol. 11 (2011) 8396-8402, https://doi.org/10.1166/jnn.2011.5081

[42] D.B. Nash, T.T. Campbell, F.E. Block, Chromium by thermal decomposition of bis(benzene)chromium, Bureau of Mines , Report Investigation 7112 April (1968)

[43] B. Bryskin, A. Kostylev, Y. Pokrovskiy, A. Lumpov, Innovative processing technology of chromium carbide coating to apprise performance of piston rings, SAE Int. J. Mater. Manf. 6(2) (2013) 131-134, https://doi.org/10.4271/2012-01-2327

[44] A. Kostylev, Y. Pokrovsky, A. Lumpov, B. Bryskin, Advanced chromium carbide coatings on piston rings by CVD: A highly adaptable new method with relatively low cost, Advanced Materials & Processes July (2012) 22-26

[45] F. Maury, A. Douard, S. Delclos, D. Samelor, C. Tendero, Multilayer chromium based coatings grown by atmospheric pressure Direct Liquid Injection CVD, Surf. Coat. Technol. 204 (2009) 983-987, https://doi.org/10.1016/j.surfcoat.2009.04.020

Tables

Table 1. Influence of the deposition temperature (T) on the structure, the atomic composition (EPMA data) and the density (RBS data) of CrC_x coatings grown by DLI-MOCVD on the inner-wall of cladding tubes, except otherwise specified. The samples (1.5 x 7 mm^2) were collected from a short section of the tube, cut transversally.

Sample	**T (°C)**	**Structure**	**Composition by EPMA (at.%)**	**Density by RBS (g/cm^3)**
CrC500	500	amorphous	$Cr_{0.62}C_{0.34}O_{0.04}$	6.9 ±0.2[a]
CrC450	450	amorphous	$Cr_{0.64}C_{0,31}O_{0.05}$	5.7 ±0.3[a]
CrC350	350	amorphous	$Cr_{0.66}C_{0.32}O_{0.02}$	6.2 ±0.2
CrC325	325	amorphous	$Cr_{0.66}C_{0.29}O_{0.05}$	6.1 ±0.2
Cr_7C_3 bulk	N/A	polycryst.	$Cr_{0.70}C_{0.30}$	6.88[b]
Cr_3C_2 bulk	N/A	polycryst.	$Cr_{0.60}C_{0.40}$	6.66[b]

[a]*The substrate was a flat Si wafer passivated with a thin amorphous SiN_x barrier layer.*
[b]*Data from PDF card 00-036-1482 (Cr_7C_3) and PDF card 00-35-0804 (Cr_3C_2)*

Table 2. Crystallization temperature under inert atmosphere (Ar) of amorphous CrC_x coatings as-deposited at 350 °C and 500 °C. The substrates used for samples deposited at 350 °C and 500 °C were a Zy-4 flat coupon and a Si wafer passivated with a thin SiN_x barrier layer, respectively. The coatings thickness was about several micrometers.

Deposition temperature (°C)	**As-deposited structure**	**Crystallization temperatures** (°C)		
		Cr_7C_3	Cr_3C_2	Cr_2O_3 *(traces)*
350	Amorphous multilayer	525 ±25	525 ±25	615 ±5
500	Amorphous monolithic	575 ±5	590 ±10	610 ±10

List of figure captions

Figure 1: SEM cross-section images of CrC_x coatings deposited on the inner-wall of Zy-4 cladding tubes between 350 °C and 500 °C.

Figure 2: SEM cross-section of CrC_x deposited on the inner-wall of Zy-4 cladding tubes at 325 °C and the corresponding EDS line scan showing the multilayers structure and composition profile.

Figure 3: Typical XRD pattern of CrC_x deposited at 450 °C. The peak position of crystalline phases Cr_7C_3 (PDF card 00-036-1482) and Cr_3C_2 (PDF card 00-35-0804) are given as reference.

Figure 4: **a.** XRD peak position of the free-C for the CrC_x coatings deposited between 325 °C and 450 °C; **b**. integrated XRD intensity ratio of free-C to the CrC_x matrix, for the CrC_x coatings deposited between 325 °C and 450 °C.

Figure 5: TEM micrograph of CrC_x coating revealing the nanocomposites microstructure formed of amorphous chromium rich regions (CrC_x matrix) and C-rich regions.

Figure 6: Raman spectrum in the 1100-1800 cm^{-1} range and its deconvolution into TPA1, D, TPA2, and G bands for the CrC coating deposited at 450 °C. The corresponding assignment for the (*) band was not possible.

Figure 7: Intensity ratio I_D/I_G of D and G bands for the CrC_x coatings deposited between 325 °C and 450 °C vs. the crystallite size L_a of graphitic clusters, according to the models of Tuinstra-Koenig and Ferrari. The dotted line indicates the transition between the amorphous carbon (a-C) and nanocrystalline graphite (nc-G) at around T=325 °C.

Figure 8: G band position (σ_G) vs. G band width (Γ_G). Our data, represented as dotted line, is compared to those for nc-G and different *a*-C taken from ref. [27].

Figure 9: SEM cross-section of CrC_x coating deposited on Zy-4 at 325 °C, annealed for 4 h at 550 °C under Ar, oxidized at 1100 °C for 15 min under ambient air and finally quenched in water at room temperature.

Figure 10: **a.** Spatial temperature profile of the deposition temperature in the longitudinal axis of the reactor for a furnace setpoint of 325 °C. **b.** Temporal variation of the deposition temperature at the beginning of the isothermal zone for a setpoint of 325 °C (point marked in green at 0.1 m from the entrance).

Figure 11: **a.** Temporal variation of the local deposition temperature in the middle of the isothermal zone for a furnace setpoint of 325 °C (point marked in blue at 0.5 m from the entrance); **b.** SEM cross-section showing the multilayer nanostructuring of a CrC_x coating grown on Zy-4 cladding near the middle of the isothermal zone for a furnace setpoint of 325 °C after a better PID tuning to mitigate the amplitude and improve the regularity of temperature oscillations.

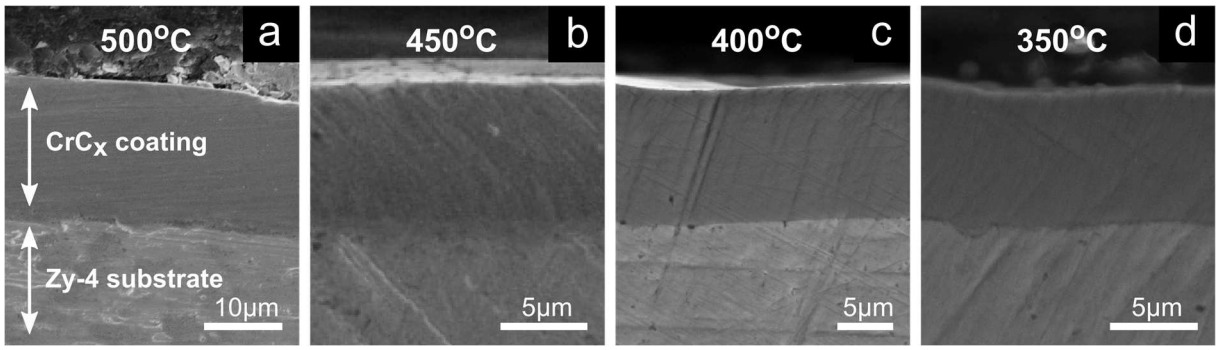
500°C
a
CrCx coating
Zy-4 substrate
10μm
450°C
b
5μm
400°C
c
5μm
350°C
d
5μm

1

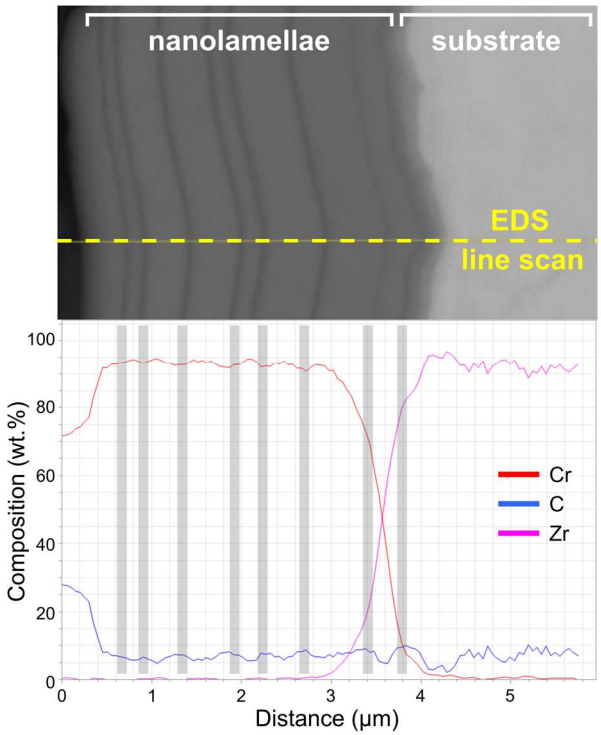
nanolamellae
substrate
EDS
line scan
Composition (wt.%)
Distance (μm)
Cr
C
Zr

2

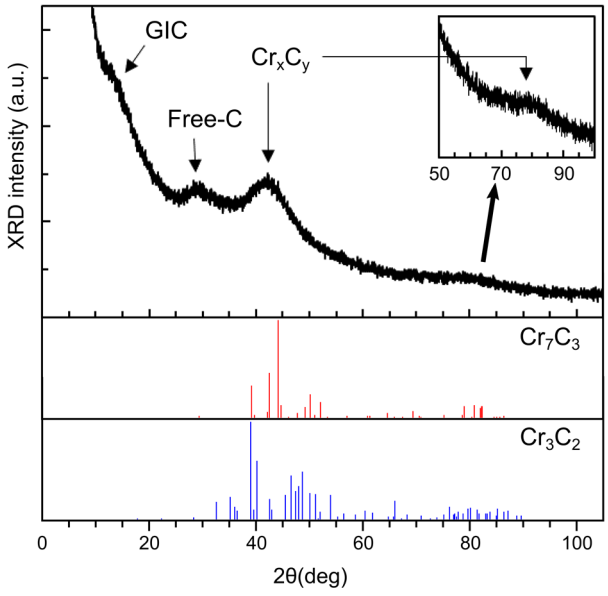
GIC
CrxCy
Free-C
XRD intensity (a.u.)
Cr7C3
Cr3C2
2θ(deg)

3

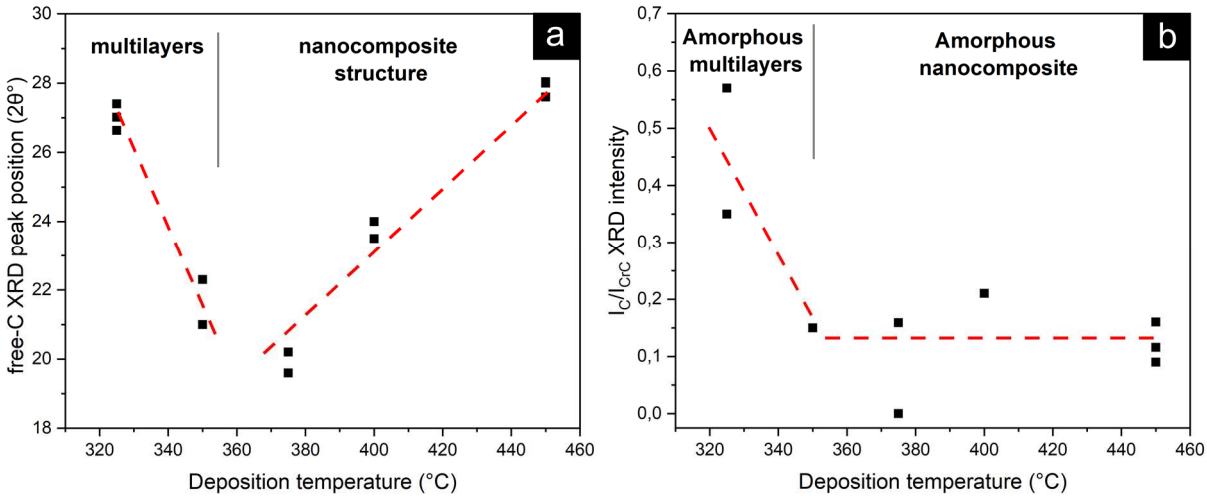
a
multilayers
nanocomposite structure
free-C XRD peak position (2θ°)
Deposition temperature (°C)
b
Amorphous multilayers
Amorphous nanocomposite
I_C/I_{CrC} XRD intensity
Deposition temperature (°C)

4

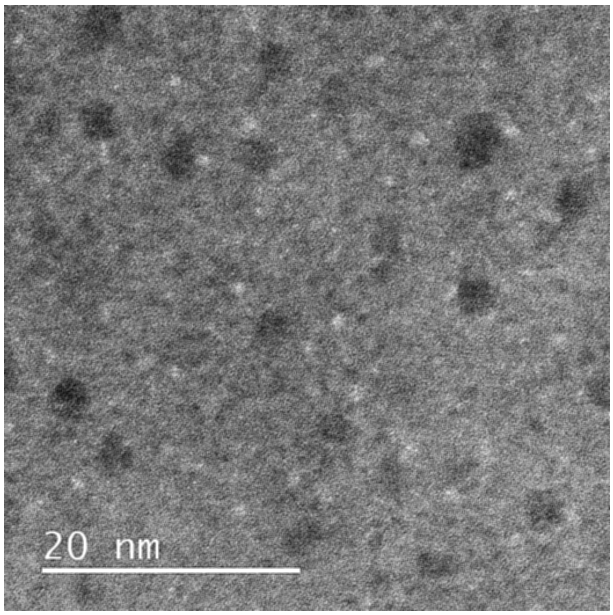
20 nm

5

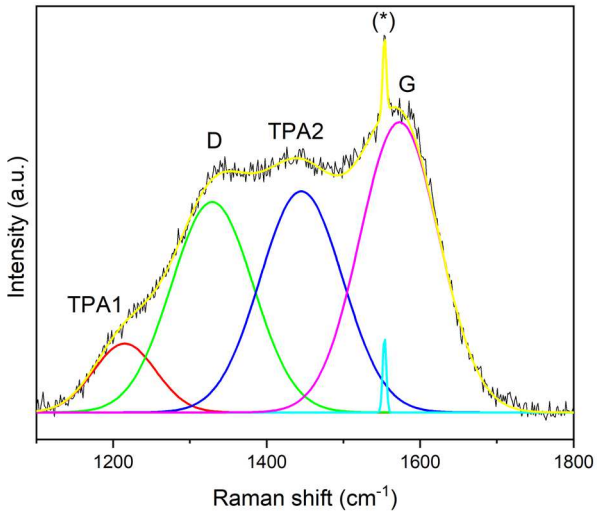
(*)
G
D
TPA2
TPA1
Intensity (a.u.)
Raman shift (cm-1)

6

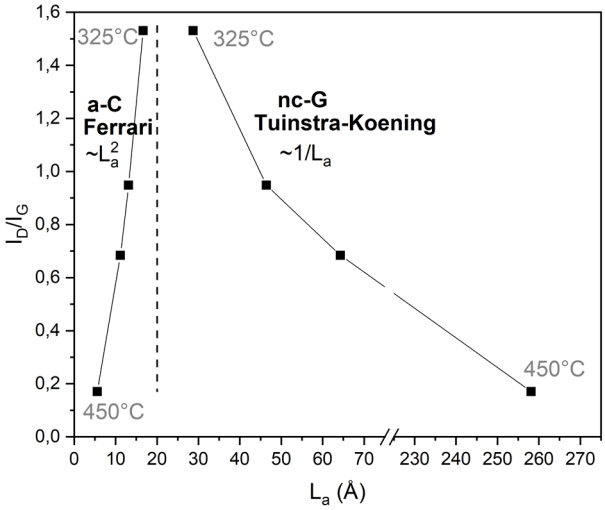

7

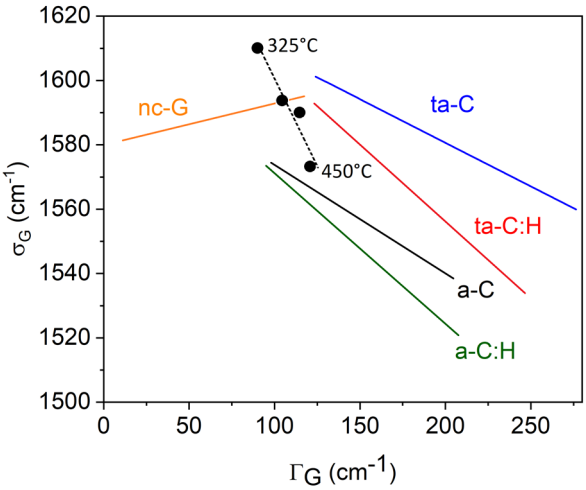

8

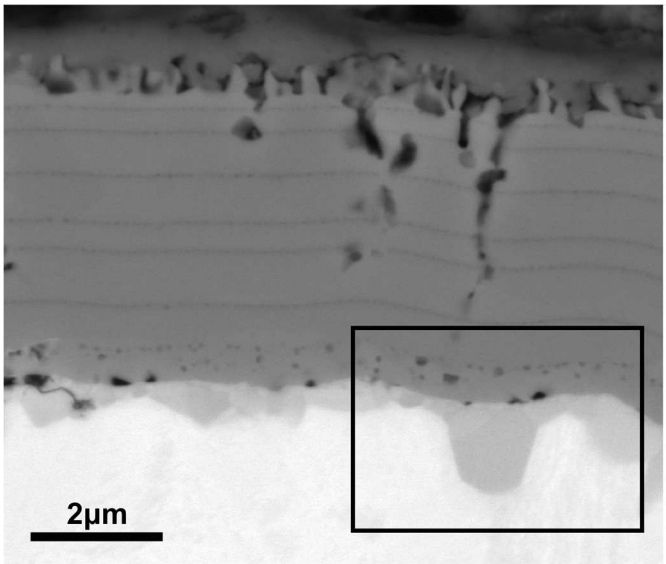

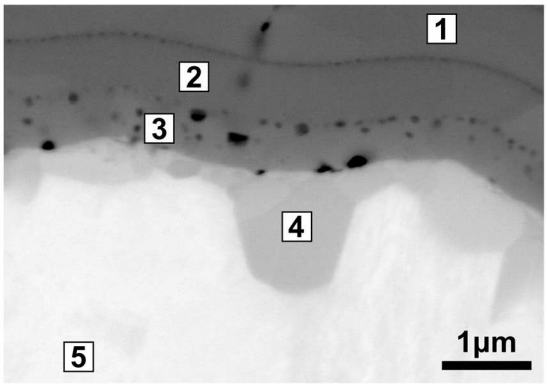

Spectrum	C	Cr	O	Zr	Other (Fe, Sn)
1	28.0	72.0			
2	27.5	72.3		0.1	
3	24.9	65.4		9.7	
4	44.8	0.9	6.3	48	
5	29.6	0.8	8.0	60.2	1.4

9

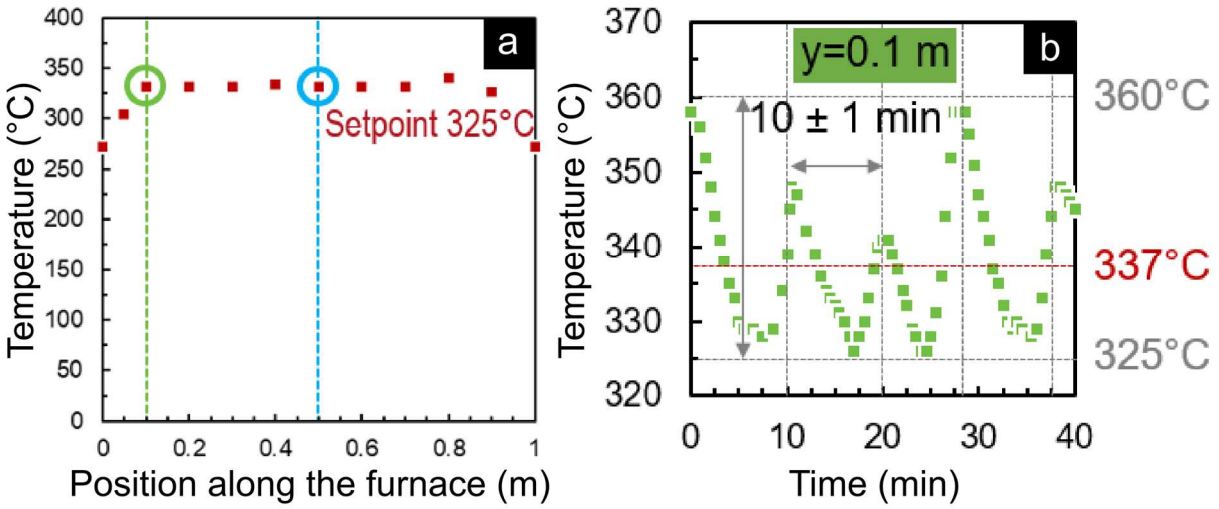
a
Temperature (°C)
Position along the furnace (m)
Setpoint 325°C
b
y=0.1 m
10 ± 1 min
360°C
337°C
325°C
Time (min)

10

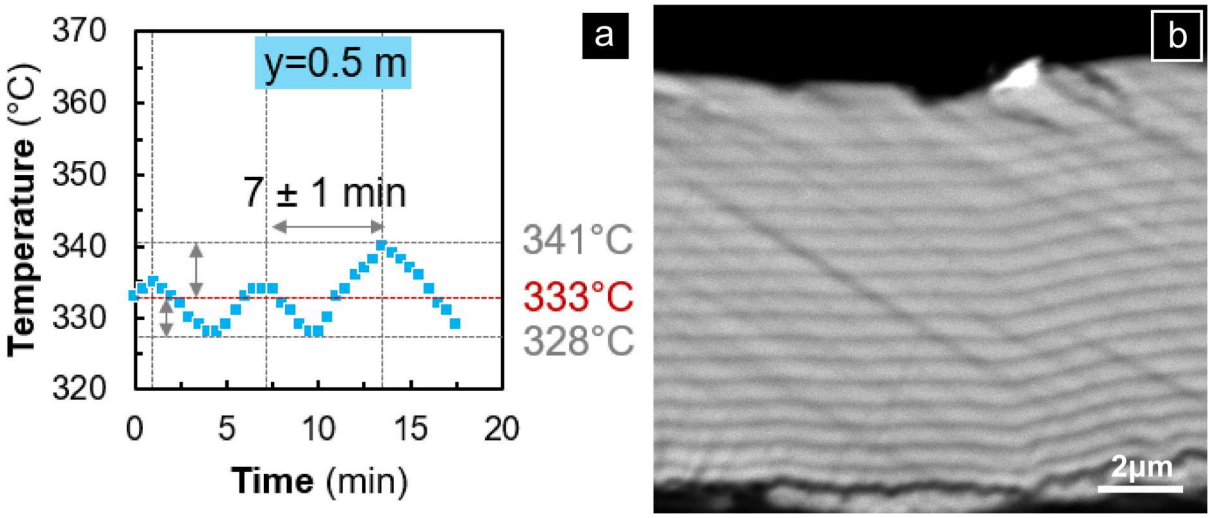
a
y=0.5 m
7 ± 1 min
341°C
333°C
328°C
Temperature (°C)
Time (min)
b
2µm